Dental Materials Journal 2019; 38(2): 303–310

Detection of enamel subsurface lesions by swept-source optical coherence tomography

Sumiyo SUZUKI[1], Yu KATAOKA[2], Masafumi KANEHIRA[3], Mikihiro KOBAYASHI[1], Takashi MIYAZAKI[2] and Atsufumi MANABE[1]

[1] *Division of Aesthetic Dentistry and Clinical Cariology, Department of Conservative Dentistry, Showa University School of Dentistry, 2-1-1 Kita-senzoku, Ohta-ku, Tokyo 145-0062, Japan*

[2] *Division of Biomaterials and Engineering, Department of Conservative Dentistry, Showa University School of Dentistry, 1-5-8 Hatanodai, Shinagawa-ku, Tokyo 142-8555, Japan*

[3] *Division of Operative Dentistry, Department of Restorative Dentistry, Tohoku University Graduate School of Dentistry, 4-1 Seiryo-machi, Aoba-ku, Sendai, Miyagi 980-8575, Japan*

Corresponding author, Sumiyo SUZUKI; E-mail: sumiyo@dent.showa-u.ac.jp

This study aimed to non-destructively analyze the progression of subsurface enamel caries using swept-source optical coherence tomography (SS-OCT), a recently developed imaging analysis modality. Artificial enamel caries at various stages of demineralization were created in bovine tooth enamel using a modified lactic acid gel system. Untreated enamel served as a control. OCT images from cross-sections of enamel were collected. Mineral density, distribution, and histological changes were analyzed using an electron probe microanalyzer, scanning electron microscopy, and contact microradiography. The Raman spectrum and X-ray structural analysis of the enamel surfaces were determined. SS-OCT detected significant differences in mineral loss among the samples. A high-brightness image was confirmed, along with changes in the respective brightness graphs proportionate to the degree of demineralization. SS-OCT can potentially be used to evaluate the progression of incipient enamel carious lesions.

Keywords: Diagnostic imaging, Dental enamel, Dental caries, Tooth demineralization, Lasers

INTRODUCTION

Early dental caries detection is a crucial step for the conservative management of demineralization. The outer layers of an initial enamel caries are fragile, and their preservation greatly controls the success or failure of remineralization therapy. The International Caries Detection and Assessment System (ICDAS) measures changes in the surface characteristics of carious lesions according to six codes (0 to 6) depending on the severity of the lesion[1]. For instance, codes 1 and 2 lesions are initial enamel carious lesions, which are primarily treated with preventive remineralization therapy[2,3], whereas code 3 lesions show localized enamel breakdown, without visual signs of dentinal involvement.

The subsurface delimiting layer of enamel can be easily destroyed, and therefore any instrumentation used near or to touch the tooth needs to be carefully handled to avoid further damage to the tissue[4]. For these reasons, tooth inspections with explorers is contraindicated[4]. On the other hand, dental X-rays have low sensitivity for an accurate diagnosis of tissue demineralization in initial enamel carious lesions[5]. Therefore, clinical diagnosis of early carious lesions relies on subjective judgments of the degree of white spot lesion formation and/or discoloration by visual clinical diagnosis.

Optical coherence tomography (OCT) is a new technique to non-invasively detect carious lesions, tooth fractures, and other intraoral lesions and restorations that can be difficult to visualize using standard dental imaging. The technique uses infrared region lasers (1,310 nm wavelength) without radiation exposure to produce cross-sectional images of the tooth. OCT acts like an optical ultrasound, and can deliver high-resolution, sub-surface images of materials that are translucent or opaque, such as teeth. OCT was first reported by Huang *et al.* at the Massachusetts Institute of Technology in 1991[6]. Since then, the clinical application of the technique has advanced rapidly[7,8]. It is now in high demand in the medical field, as it offers better resolution images than magnetic resonance imaging (MRI) or computed tomography (CT).

The earliest form of OCT was time-domain OCT (TD-OCT), and this technique was limited by its scanning speed, measuring light echoes one at a time. These limitations led to the development of Fourier-domain OCT (FD-OCT)[9-11], first used in 1995, which did not require physical scanning and was much faster than TD-OCT. FD-OCT removed motion artifacts by measuring the oscillation wavelength of the laser light source using a spectrometer, with a sensitivity 10- to 100-times that of TD-OCT[8]. The technique was further improved with the advent of swept-source OCT (SS-OCT), which sought to incorporate the advantages of the different OCT methods, offering a fast frequency while sweeping an oscillation wavelength and measuring the interference signal in terms of time. In FD-OCT, movement of the camera causes a fringe washout of the

Color figures can be viewed in the online issue, which is available at J-STAGE.

Received Nov 21, 2017: Accepted Jul 3, 2018
doi:10.4012/dmj.2017-404 JOI JST.JSTAGE/dmj/2017-404

picture because of the low sensitivity for infrared light. This issue was resolved with SS-OCT, as a CCD camera was not required, with little decrement of the signal intensity due to depth changes. SS-OCT therefore offers superior sensitivity over other CT modalities, providing high-resolution images with an approximate sensitivity of 10 μm longitudinally and 30 μm laterally in the air; by comparison, general medical CT and dental CT have sensitivities of 240 to 600 μm[12] and approximately 100 μm[13], respectively.

Several OCT devices have been used for dentistry over the years[14-16]. SS-OCT has various applications in observing naturally occurring lesions, including enamel fissures, incipient enamel caries, and enamel white spot lesions[17-21]. The outer surface of the enamel is continuously cycling between demineralization and remineralization, and when this balance is disrupted, demineralization will progress and the tooth substance will be compromised[22]. In the early stages of enamel caries formation, the outer layer collapses first in response to damage, such as external pressure. Hence, early and accurate detection using non-invasive imaging techniques could help to avoid further tooth deterioration. In addition, enamel remineralization treatments have attracted attention in recent years[23,24]. Therefore, enamel remineralization following an early diagnosis using SS-OCT has clinical utility. However, as yet, no study has investigated the changes that occur during incipient enamel caries formation using SS-OCT. The purpose of this study was to examine the progression of artificial demineralization nondestructively by measuring early enamel changes using SS-OCT.

MATERIALS AND METHODS

Specimen preparation

This study was approved by the local ethics committee of the Institute of Laboratory Animals of Showa University School of Dentistry, Tokyo, Japan (approval number D8017). Eight sound bovine incisors, without any visible alterations, were frozen after extraction and used in this study. Three block specimens (4×5×4 mm) were cut from the buccal enamel surfaces of the bovine incisors using a low-speed diamond saw (Isomet, Buehler, Lake Bluff, IL, USA, Fig. 1A; small squares). The enamel surface was sequentially flattened using waterproof polishing carbide paper (Silicon carbide, Riken corundum, Saitama, Japan) from 600 to 1500 grit under running water. The specimens were rinsed with pure distilled water thoroughly, and then ultrasonicated in pure distilled water three times for 5 min. The specimens were blotted dry and then coated with an acid-resistant varnish, leaving an exposed window of enamel of approximately 2×3 mm.

Demineralization procedures

Specimens were randomly allocated to three experimental groups and a control group. In the three experimental groups, bovine enamel subsurface lesions were created using a modified lactic acid gel

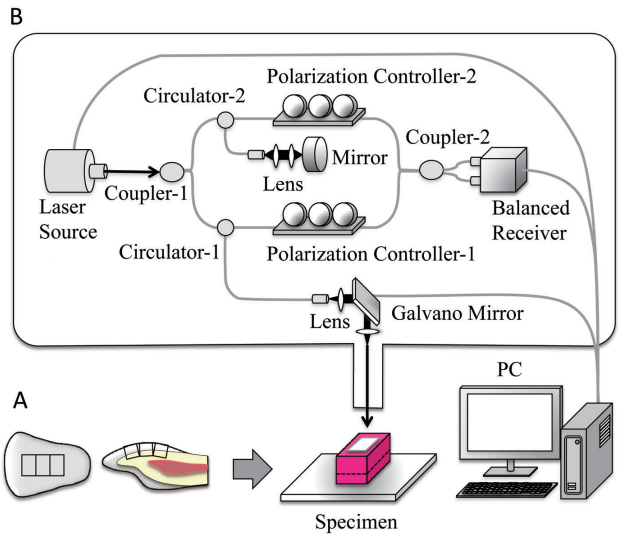

Fig. 1 Specimens and SS-OCT.
(A) Three block specimens (4×5×4 mm) were cut from the buccal enamel surfaces of bovine incisors. Each specimen is indicated by a square box. (B) Diagram of the SS-OCT set up. The experimental SS-OCT system consists of a laser as a light source, an interferometer, a probe with mirror, and a personal computer system. The frequency of the driving signal was set to 50 kHz, and a filter scanning range at 140 nm.

system, following the method previously reported by Ingram and Silverstone[25] and Hayashi[26]. Briefly, three specimens were placed at the bottom of a cylindrical plastic container with the test surfaces facing up and immersed in one of three volumes of 8% methylcellulose gel (MCgel; Methocel MC, Fluka, Buchs, Switzerland) at 37°C for 24 h: Sub-L samples were immersed in 50 mL MCgel; Sub-M samples in 45 mL; and Sub-H samples in 40 mL (n=6). A piece of filter paper was placed on top of the gel and then all samples were covered with 70 mL of 0.1 M lactic acid, pH 4.6. White spot enamel subsurface lesions were simulated in the lactic gel system over 10 days at 37°C. Specimens were thoroughly rinsed with pure distilled water to remove the MCgel, and stored in artificial saliva (1.5 mM $CaCl_2$, 0.9 mM KH_2PO_4, 20 mM Hepes, 150 mM NaCl, pH 7.0 at 37°C)[26] that was refreshed daily. For the control group, untreated enamel bovine specimens were stored in artificial saliva.

OCT imaging of the specimens

Yoshida dental OCT (YOSHIDA, Tokyo, Japan) is the SS-OCT prototype that was used in this study (Fig. 1B). Before scanning, the specimens were removed from the artificial saliva and washed with pure distilled water. Visible droplets of water were blotted, with negligible moisture on the surface. Blotting —rather than completely drying— prevented the surface from showing signs of dehydration[27]. Specimens were then placed on a metal table with the experimental surface facing up (Fig.

1A). The scanning beam was operated at 1,310 nm center wavelength oriented approximately 90° to the surface. A central 3-mm rectangular area on the experimental surface was used for cross-sectional scanning. The parameters were fixed at a contrast of 91, a width level of 100, and a gamma level of 0.16. The resolution was 11 μm (axial) and 30 μm (horizontal) in air. The OCT data are shown as absolute values, with no revision of the 256 shades of gray images. Fourier transformation was applied to the detector signal and the vertical axis shows the logarithmic Fourier-transformed values of intensity. In this study, the unit of the vertical axis is arbitrary units (a.u.).

SEM observation and elemental analysis (cross section)
Three specimens were dehydrated in an ethanol series, and then embedded in epoxy resin (Technovit 4006, Heraeus Kulzer, Hanau, Germany). From each specimen, two blocks were cut centrally and parallel to the tooth axis on the long side (Fig. 1A). One of the blocks was polished with a gamma alumina polishing paste (grain diameter, 0.05 μm) and then sputter-coated with gold. For morphological observation, cross-sections of the block were analyzed using a wavelength-dispersive X-ray spectroscopy electron probe microanalyzer (EPMA) with an image observation function (EPMA-1600/1610, Shimadzu, Kyoto, Japan), and was used for field-emission scanning electron microscopy (FE-SEM; S-4700, Hitachi, Tokyo, Japan).

Measurement of the mineral density by contact microradiography (CMR)
The second block was cut into 500-μm-thick sections perpendicular to the enamel surface using a diamond saw (Isomet, Buehler), and polished to 100-μm-thin sections using silicon carbide (SiC) papers (Riken Corundum) of 600 to 1500 grit under running water. To confirm the generation of enamel lesions at the cross section, each section was radiographed on film (Professional Special Holographic Film SO-181, Kodak, Tokyo, Japan) using CMR at 11 kV and 2 mA for 10 min (SOFRON SRO-M50, Sofron, Tokyo, Japan). Radiographic images taken with an optical microscope were digitized and analyzed with dedicated computer software (ImageJ 1.45l, NIH, Bethesda, MD, USA). Mineral profiles were created by digital gray-scale values of 256 gradations; the information analyzed was obtained from an area of approximately 70 μm (width) from the center of the enamel surface to a depth of approximately 300 μm. Mineral loss value (ΔZ, vol%×μm) was computed using the area obtained by plotting the volume percent mineral profile of the enamel depth for each section of the subsurface lesion, with sound untreated enamel set as 100 vol% mineral, and regions of the slide without tissue set as 0 vol%.

Statistical analysis
Mineral loss (ΔZ) in each subsurface lesion group (Sub-L, Sub-M, Sub-H) was compared using a one-way ANOVA followed by Tukey's *post-hoc* tests. Calculations were performed using SPSS23J (Windows, IBM, Armonk, NY, USA), with significance set to 5%.

Surface characterization
Each specimen from the Sub-L, Sub-M, Sub-H and Control groups, which had been stored in artificial saliva, was rinsed with pure distilled water and dried. The enamel surface was analyzed using micro Raman spectroscopy (RXN1, Kaiser Optical Systems, Ann Arbor, MI, USA) with a near-infrared (785 nm) laser and an integration time of 20 s with three co-additions. The crystalline phases of the enamel surface of the Control group and Sub-L group were identified by X-ray diffraction (XRD; XRD-6100, Shimadzu) with CuK α radiation.

RESULTS

Imaging and brightness graphs from SS-OCT
Figure 2 shows a representative example of an SS-OCT

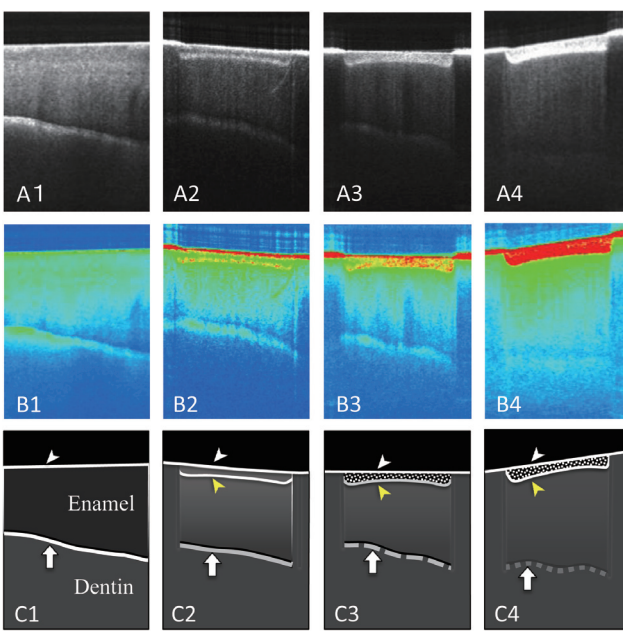

Fig. 2 SS-OCT images and illustrations.
(A) SS-OCT images, (B) SS-OCT color images, and (C) An illustrative representation of what is shown in the images. Column 1 is the control (A1, B1, C1), followed by enamel with the different subsurface lesions (column 2, Sub-L; column 3, Sub-M; column 4, Sub-H). The polished surface is indicated by a white arrowhead. A yellow arrowhead indicates the second high-brightness line, which appears between the sound enamel and areas of demineralization. In the color image, the polished enamel surface is red, and it indicates the brightness limit of the color image; the second line (yellow line) indicates a lower level of brightness. The DEJ is detected as a white line (white arrows). The DEJ is clearly observed at the border of the enamel and the dentine in the Control group.

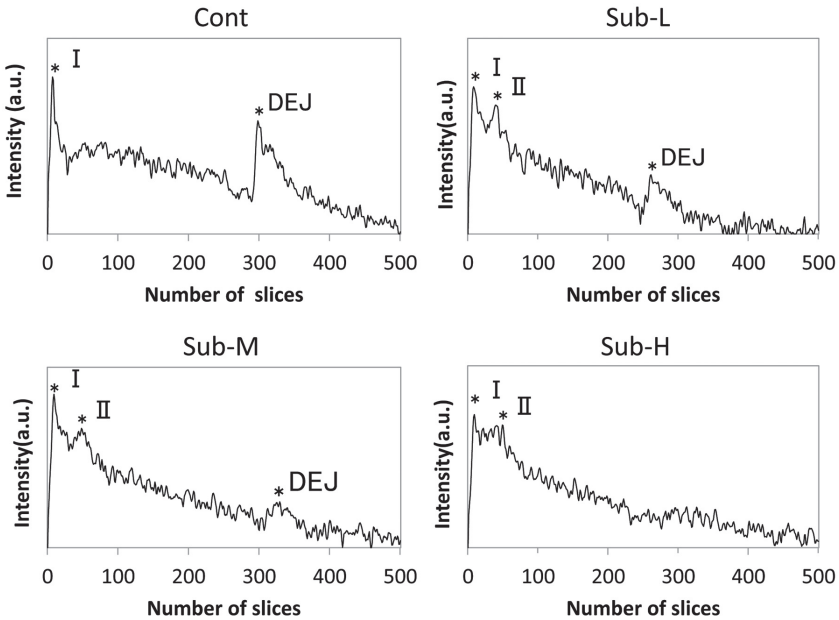

Fig. 3 SS-OCT signal intensity of the enamel surface area.
The first peak indicates the polished enamel surface (*I). The second peak appears at the border between the demineralization area and the sound enamel (*II). The first and second peaks, respectively, are indicated a white arrowhead and a yellow arrowhead (see Fig. 2).

image. In the Sub-L group (column 2), a second line of significant brightness appears between the enamel surface and the dentin-enamel junction (DEJ; yellow arrowhead, Figs. 2 C2–C4). In the Sub-M group (column 3), there is an increase in brightness between the surface and second bright line (yellow arrowhead), whereas, in the Sub-H group, the distinction between the two lines is lost. Brightness, as an indicator of the subsurface lesion, was highest in the Sub-H group as compared with the Sub-L and Sub-M groups. As demineralization proceeds, the brightness of the surface increases, and the line of the DEJ is blurred.

Figure 3 shows the brightness graphs for each group derived from the SS-OCT data. In the Sub-L group, two peaks (asterisks) were detected, with the second peak lower than the first peak. The wave-form of the DEJ was clear. In the Sub-M group, multiple small waves were detected between the first peak and the small second peak. In the Sub-H group, numerous waves were found between the first and second peaks, and the DEJ peak was not discernable. The DEJ peak tends to become unclear as demineralization progresses.

FE-SEM image and EPMA

We next used SEM (Fig. 4A) to identify any differences in the contrast of the samples. Samples in the Sub-L group were predominantly free from any visible defect, whereas clear deficiencies in the tooth substance were observed in the subsurface lesions for samples in the Sub-M and Sub-H groups. We also found a decrease in Ca and P in these sub-groups with the EPMA (Fig. 4A). Where SEM showed changes in the contrast level among the different test groups, there also tended to be a decrease in the levels of Ca and P in the EPMA analysis.

Figure 4B shows the formation of an enamel rod around the defect, with extended gaps found between the enamel rods in the Sub-M group.

Mineral profile

Statistically significant differences were found among the treatment groups in terms of mineral loss (ΔZ) ($p<0.05$): 4,043.8±642.0 (vol%×μm) in the Sub-L group, 5,636.1±490.1 in the Sub-M group, and 8,573.7±1,081.6 in the Sub-H group (Figs. 4C and D).

Raman spectroscopy and XRD analysis

We next used Raman spectroscopy and XRD to ascertain the composition of the treated samples as compared with the Control. A Raman scattering peak for PO_4^{3-} was detected in all groups: ν 1 (960 cm^{-1}), ν 2 (430 cm^{-1}), ν 3 (1,044 cm^{-1}), and ν 4 (591 cm^{-1}) (Fig. 5A). Figure 5B compares the representative XRD results for the Control and Sub-L groups only. Even though the analysis pattern showed the same shape for both the Sub-L and Control groups, we measured a reduction in the diffraction intensity for the Sub-L group. For both groups, the maximum diffraction peak was detected at 32°, which is indicative of hydroxyapatite.

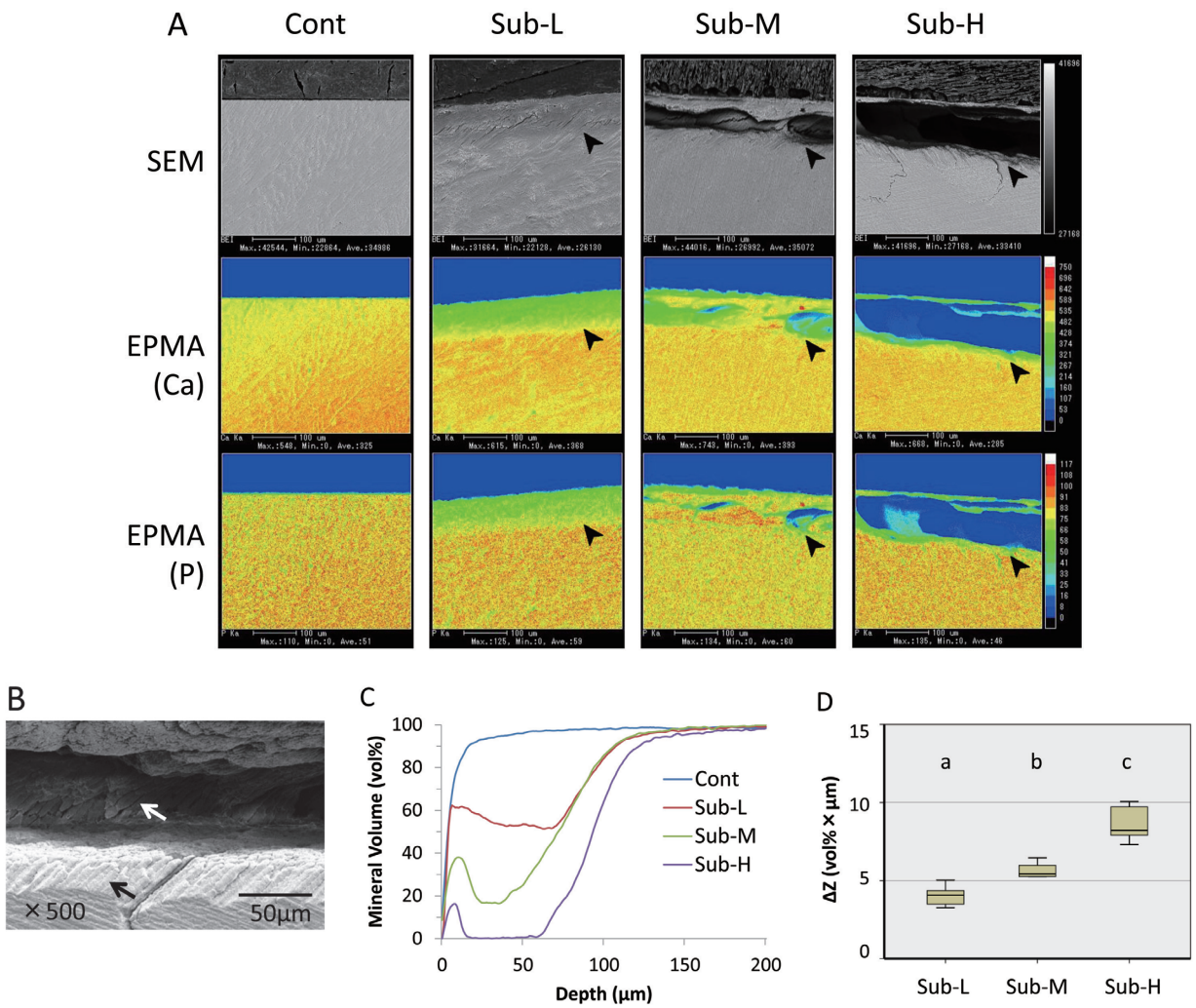

Fig. 4 Representative photographs of SEM and wavelength-dispersive X-ray spectroscopy EPMA. (A) A black arrowhead indicates the border of the sound enamel and the demineralized lesion. Distributions of calcium (Ca) and phosphorus (P) in the enamel were measured using the element line scan at an accelerating voltage of 15 kV, and a beam current of 0.05 μA. Ca and P elution from under the enamel surface increased as demineralization progressed. Although the demineralization depth tended to deepen with increased demineralization, lesions of approximately 100 μm were measured beneath the surface. (B) FE-SEM photographs of the demineralized subsurface area in the Sub-M group. A black arrow indicates the sound enamel structures where the enamel rods are ordered regularly, whereas a white arrow indicates the irregularity of enamel rods in the demineralized region. (C) Average mineral profiles of sound enamel (Cont) and subsurface regions (Sub-L, Sub-M, Sub-H). (D) Intergroup comparisons of mineral loss value (Δ*Z*, vol%×μm). Different lower-case letters denote significantly different groups.

DISCUSSION

In OCT, infrared lasers are reflected to provide an image of the irradiated subject. Where the internal structure of the subject is heterogenous, there are differences in how the light is reflected, which generates an image. Enamel is composed of 96% inorganic mineral in the form of hydroxyapatite crystals, with a very small amount of organic matrix around each crystal structure[28,29]. By comparison, dentin is composed of approximately 70% hydroxyapatite crystals[30]. These histological differences appear as differences in reflectivity and this allows for discrimination between enamel and dentin in an image.

The DEJ of the human tooth is an undulating structure[31], and light scattering from this region likely explains why the DEJ is observed as a bright, undulating white line (Fig. 2). Previous reports have shown that caries and white spots are depicted as increased brightness at the site but also show a decrease in brightness beneath the enamel lesion[18-20]. Further, it has been reported that the attenuation coefficient of the infrared region laser changes with the progression

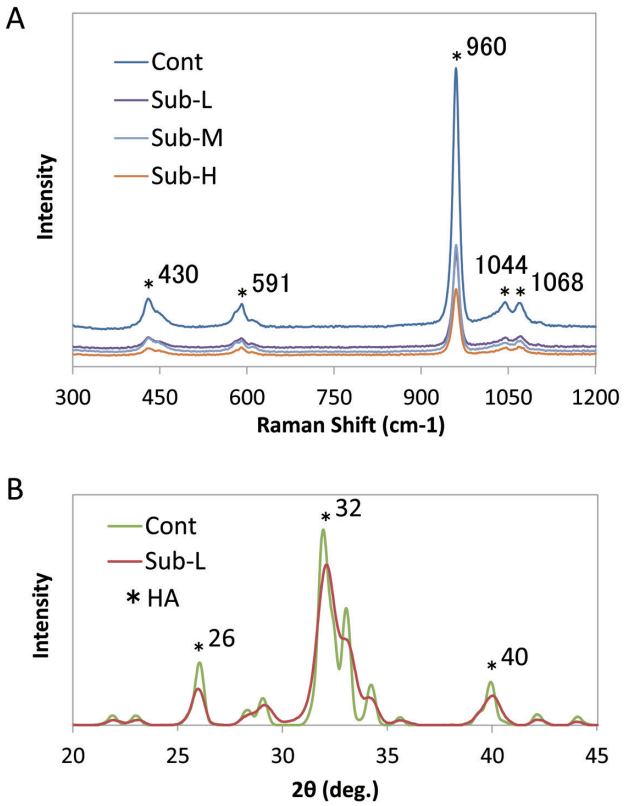

Fig. 5 Micro Raman spectroscopy and pattern of XRD. (A) The Raman spectra of sound enamel (Cont) and treated enamel (Sub-L, Sub-M, Sub-H) were acquired with a Raman probe with a near-infrared (785 nm) laser excitation and an integration time of 20 s with three co-additions. The dispersion intensity (ν 1 at 960 cm^{-1}) was the strongest and showed a symmetrical peak. Two peaks were detected in ν 2: a major peak at 430 cm^{-1} and gentler wave form at 445 cm^{-1}. Two peaks were also detected in ν 3a: a major peak at 1,068 cm^{-1}, and a strong, asymmetrical peak at 1,044 cm^{-1}. Finally, three peaks were clearly visible in ν 4: a major peak at 591cm^{-1}, a gentler wave at 580 cm^{-1}, and a minor peak at 608 cm^{-1}. Raman signal intensity of the enamel surface decreased as demineralization progressed. No significant change in peak position was observed, but the width of the peak increased. These changes indicate impaired enamel crystallinity. (B) XRD. The asterisk indicates 3 typical peaks of hydroxyapatite (HA). These three peaks are in the same position for the control (Cont) group and Sub-L group. The Sub-L group shows broader diffraction peaks of poor crystallinity as compared with the Cont group.

of demineralization and decreases the detection of the depth direction[32]. Thus, the DEJ is not detected clearly when surface enamel is demineralized. This offers an important first clue as to the presence of an initial enamel caries lesion or a crack and can help to quickly confirm the stage of deterioration. In this study, as demineralization proceeds, the brightness of the surface increases, and the line of the DEJ is blurred. There was no diffused reflection and little decrement in the laser beam in the Sub-L group samples, which show a low degree of demineralization; in these cases, the laser light appears to reach the DEJ. As demineralization progresses, an increasing number of defects in the demineralized zone begins to affect the laser beam path, and this makes it gradually more difficult to interpret the results.

During the early stages of enamel caries formation, the surface of the enamel becomes rough, and a small lesion is created through demineralization at the subsurface. The interface between the enamel rod and the interrod enamel —which is poorly mineralized— is preferentially dissolved by acid erosion. From there, the acid spreads through the gap[29,33]. In this study, we observed extended gaps between the enamel rods (Fig. 4B), which presumably became the invasion course for the acid. The demineralized enamel surface of the initial caries was rough, with numerous depressions found[29]. In the mineral profile of each group (Fig. 4C), we noted an upstroke in the graph —indicating the enamel surface— and a decrease in mineral density with further demineralization. There were statistically significant differences among the treatment groups in terms of mineral loss (ΔZ), which was highest in the Sub-H group, followed by the Sub-M group and then the Sub-L group. Results from the Raman spectroscopic analysis (Fig. 5A) indicated that the signal intensity of each sub-group decreased monotonically as compared with the Control group. Dissolution of the apatite crystals caused an increase in surface microasperities, which, in turn, increased the amount of free PO_4^{3-} and lateral light scattering. In this study, we systematically created three grades of subsurface lesions, and the results indicate that we succeeded in achieving three levels of demineralization.

Using SS-OCT imaging, we identified a bright line at top of the image in all groups (Fig. 2) and a peak in the brightness graph (Fig. 3). These findings suggest preservation of the enamel surface under all conditions. Furthermore, a second bright line was observed at the border of the demineralization layer and the normal tissue (as inferred from the EPMA analysis; Fig. 2) in the Sub-L group, and a corresponding second peak in brightness graph (Fig. 3). Therefore, we assume that the image detected crystal dissolution that occurred before parenchymatous defects were made by demineralization. Previous studies have found a correlation between the local refractive index and the mineral content (density) of the enamel[34]. In this study, we presume that the appearance of a bright line at the border of the normal tissue occurs because of the reflection resulting from a decrease in the refractive index produced by demineralization in the subsurface lesions (Fig. 4A). In the Sub-L group, because only the second bright line could be confirmed clearly, there seemed to be no other factors that could induce laser dynamic scattering in the demineralization layer between the first and second

bright lines. During initial enamel caries formation, the organic matrix between the hydroxyapatite crystals is also dissolved and leaves irregularly shaped enamel nanorods and numerous pores of roughly 100 nm in size at the subsurface[29]. This additional porosity affects the invasion route of the acid[29,35]. Through XRD analysis (Fig. 5B), the diffraction intensity decreased in the Sub-L samples during early demineralization. The density of the hydroxyapatite crystals at the side of the abrasion was low, and there was disorder among the crystals. However, the resolution of SS-OCT used in this study may not be able to detect nano-porosities of the demineralized enamel that appear between the apatite crystals, and this may explain why the image displays as one bright line (the second line) of differing thicknesses in the Sub-L group. The progression of demineralization between the Sub-L and Sub-M groups was gradual in the osculum of the subsurface lesion of the cavity (from nano-porosities to micro-defect; Fig. 4A). With SEM (Fig. 4A), we observed a cavity under the enamel and obvious demineralization in the adjacent layers. These findings are similar to the results of others, who showed progressive demineralization of the surface layer[29]. Because SS-OCT captures the cavities as an image, the light that reflects within the defect between the surface and second bright line appears as a fairly bright region on the image for the Sub-M group, and an even brighter region on the image for the Sub-H group, which showed higher rates of demineralization. Demineralization in the Sub-H group reached the level of code 3 (ICDAS), which describes localized enamel breakdown, without the clinical visual signs of dentinal involvement. However, a surface layer was still observed in the Sub-H group: this may explain why a lesion progresses so quickly to this stage of demineralization, with most of the lesion occurring beneath the surface. Furthermore, we controlled for any external influences, such as pressure, in this study, which could additionally affect the rate of decay. It was only through SS-OCT that we could observe non-invasively the hollowing and loss of demineralization under the enamel surface. These histological changes were supported by changes in the brightness graphs.

CONCLUSION

In this study, we show that the recently developed SS-OCT can evaluate changes in tooth mineral dynamics within subsurface lesions. We objectively and non-invasively measured weakening of the tooth substance, which begins as crystal dissolution. Whereas OCT provides a means to explore the histological changes occurring under the enamel surface, SS-OCT allows us to detect incipient caries as a slight bright line at the border of the normal tissue. Our findings show the benefits of using SS-OCT in dental practice to determine the type of intervention required to protect and preserve the existing enamel. SS-OCT may foreseeably provide superior, clearer imaging of concealed tooth demineralization and help to evaluate tooth conditions that cannot be determined using other conventional methods.

ACKNOWLEDGMENTS

We are grateful to Professor Akira SENDA, Professor Morioki FUJITANI and Associate professor Maki HAYASHI in the Department of Conservative Dentistry, School of Dentistry, AICHI GAKUIN UNIVERSITY for helpful discussions about the enamel subsurface lesions created using a modified lactic acid gel system.

This study was supported in part by grants for research received from THE YOSHIDA DENTAL MFG, Japan.

The authors declare no potential conflicts of interest with respect to the authorship and/or publication of this article.

REFERENCES

1) Ismail AI, Sohn W, Tellez M, Amaya A, Sen A, Hasson H, Pitts NB. The international caries detection and assessment system (ICDAS): an integrated system for measuring dental caries. Community Dent Oral Epidemiol 2007; 35: 170-178.
2) American Dental Association Council on Scientific Affairs. Professional applied topical fluoride; Evidence-based clinical recommendations. J Am Dent Assoc 2006; 137: 1151-1159.
3) Agrawal N, Pushpanjali K. Feasibility of including APF gel application in a school oral health promotion program as a caries- preventive agent: a community intervention trial. J Oral Sci 2011; 53: 185-191.
4) Kühnisch J, Dietz W, Stösser L, Hickel R, Weltzien RH. Effects of dental probing on occlusal surfaces —A scanning electron microscopy evaluation. Caries Res 2007; 41: 43-48.
5) Schwendicke F, Tzschoppe M, Paris S. Radiographic caries detection: A systematic review and meta-analysis. J Dent 2015; 43: 924-933.
6) Huang D, Swanson EA, Lin CP, Schuman JS, Stinson WG, Chang W, Hee MR, Flotte T, Gregory K, Puliafito CA, Fujimoto JG. Optical coherence tomography. Science 1991; 254: 1178-1181.
7) Swanson EA, Izatt JA, Hee MR, Huang D, Lin CP, Schuman JS, Puliafito CA, Fujimoto JG. In vivo retinal imaging by optical coherence tomography. Opt Lett 1993; 18: 1864-1866.
8) Nioka S, Chen Y. Optical tecnology developments in biomedicine: history, current and future. Transl Med UniSa 2011; 1: 51-150.
9) De Boer JF, Cense B, Park BH, Pierce MC, Tearney GJ, Bouma BE. Improved signal-to-noise ratio in spectral-domain compared with time-domain optical coherence tomography. Opt Lett 2003; 28: 2067-2069.
10) Leitgeb R, Hitzenberger CK, Fercher AF. Performance of fourier domain vs. time domain optical coherence tomography. Opt Express 2003; 11: 889-894.
11) Wojtkowski M, Srinivasan V, Fujimoto JG, Ko T, Schuman JS, Kowalczyk A, Duker JS. Three-dimensional retinal imaging with high-speed ultrahigh-resolution optical coherence tomography. Ophthalmology 2005; 112: 1734-1746.
12) Kampschulte M, Langheinirch AC, Sender J, Litzlbauer HD, Althöhn U, Schwab JD, Alejandre-Lafont E, Martels G, Krombach GA. Nano-computed tomography: technique and applications. Rofo 2016; 188: 146-154.
13) Kiljunen T, Kaasalainen T, Suomalainen A, Kortesniemi M. Dental cone beam CT: A review. Phys Med 2015; 31: 844-860.
14) Iino M, Murayama R, Shimamura Y, Kurokawa H, Furuichi

T, Suzuki T, Miyazaki M. Optical coherence tomography examination of the effect of S-PRG filler extraction solution on the demineralization of bovine enamel. Dent Mater J 2014; 33: 48-53.
15) Jones RS, Fried D. Remineralization of enamel caries can decrease optical reflectivity. J Dent Res 2006; 85 :804-808.
16) Chan KH, Chan AC, Fried WA, Simon JC, Darling CL, Fried D. Use of 2D images of depth and integrated reflectivity to represent the severity of demineralization in cross-polarization optical coherence tomography. J Biophotonics 2015; 8: 36-45.
17) Hsieh YS, Ho YC, Lee SY, Chuang CC, Tsai JC, Lin KF, Sun CW. Dental optical coherence tomography. Sensors 2013; 13: 8928-8949.
18) Nakagawa H, Sadr A, Shimada Y, Tagami J, Sumi Y. Validation of swept source optical coherence tomography (SS-OCT) for the diagnosis of smooth surface caries in vitro. J Dent 2013; 41: 80-89.
19) Espigares J, Sadr A, Hamba H, Shimada Y, Otsuki M, Tagami J, Sumi Y. Assessment of natural enamel lesions with optical coherence tomography in comparison with microfocus x-ray computed tomography. J Med Imaging 2015; 2: 014001.
20) Ibusuki T, Kitasako Y, Sadr A, Shimada Y, Sumi Y, Tagami J. Observation of white spot lesions using swept source optical coherence tomography (SS-OCT): in vitro and in vivo study. Dent Mater J 2015; 34: 545-552.
21) Shimada Y, Sadr A, Sumi Y, Tagami J. Application of optical coherence tomography (OCT) for diagnosis of caries, cracks, and defects of restorations. Curr Oral Health Rep 2015; 2: 73-80.
22) Featherstone JDB. The continuum of dental caries-evidence for a dynamic disease process. J Dent Res 2004; 83: C39-42.
23) Tanaka R, Shibata Y, Manabe A, Miyazaki T. Mineralization potential of polarized dental enamel. PLoS One 2009; 4: e5986.
24) Ogura K, Tanaka R, Shibata Y, Miyazaki T, Hisamitsu H. 2013. In vitro demineralization of tooth enamel subjected to two whitening regimens. J Am Dent Assoc 2013; 144: 799-807.
25) Ingram GS, Silverstone LM. A chemical and histological study of artificial caries in human dental enamel in vitro. Caries Res 1981; 15: 393-398.
26) Hayashi M. Characteristic changes of enamel surface layer following demineralization of remineralized enamel subsurface lesion. Jpn J Conserv Dent 2012; 55: 398-410.
27) Nazari A, Sadr A, Campillo-Funollet M, Nakashima S, Shimada Y, Tagami J, Sumi Y. Effect of hydration on assessment of early enamel lesion using swept-source optical coherence tomography. J Biophotonics 2013; 6: 171-177.
28) Sui T, Sandholzer MA, Baimpas N, Dolbnya IP, Landini G, Korsunsky AM. Hierarchical modelling of elastic behaviour of human enamel based on synchrotron diffraction characterization. J Struct Biol 2013; 184: 136-146.
29) Chung HY, Huang KC. Effects of peptide concentration on remineralization of eroded enamel. J Mech Behav Biomed Mater 2013; 28: 213-221.
30) Xu C, Yao X, Walker MP, Wang Y. Chemical/molecular structure of the dentin-enamel junction is dependent on the intratooth location. Calcif Tissue Int 2009; 84: 221-228.
31) Whittaker DK. The enamel-dentine junction of human and Macaca irus teeth: a light and electron microscopic study. J Anat 1978; 125: 323-335.
32) Mandurah MM, Sadr A, Shimada Y, Kitasako Y, Nakashima S, Bakhsh TA, Tagami J, Sumi Y. Monitoring remineralization of enamel subsurface lesions by optical coherence tomography. J Biomed Opt 2013; 18: 046006.
33) Frank RM. Structural events in the caries process in enamel, cementum, and dentin. J Dent Res 1990; 69: 559-566.
34) Hariri I, Sadr A, Nakashima S, Shimada Y, Tagami J, Sumi Y. Estimation of the enamel and dentin mineral content from the refractive index. Caries Res 2013; 47: 18-26.
35) LeGeros RZ. Chemical and crystallographic events in the caries process. J Dent Res 1990; 69: 567-574.